

# Comparison of MGS TES FFSM eddies and MOC storms, MY 24–26

John Noble<sup>1,2</sup>, Robert M. Haberle<sup>2</sup>, Alison F. C. Bridger<sup>1,2</sup>, R. John Wilson<sup>3</sup>,  
Jeffrey R. Barnes<sup>4</sup>, Jeffrey L. Hollingsworth<sup>2</sup>, Melinda A. Kahre<sup>2</sup>, Bruce Cantor<sup>5</sup>

1. San Jose State University, 2. NASA/Ames Research Center, 3. NOAA Geophysical Fluid Dynamics Laboratory, 4. Oregon State University, 5. Malin Space Science Systems



San José State  
UNIVERSITY

## Introduction

Mars Global Surveyor (MGS) orbiter observed a planet-encircling dust storm (PDS) in Mars year (MY) 25 from  $L_s=176.2\text{--}263.4^\circ$  Cantor (2007). We have integrated and examined all available MGS data in order to better understand and characterize the dynamical processes responsible for MY 25 PDS initiation and expansion (Haberle *et al.* 2005; Noble *et al.* 2006; Wilson *et al.* 2008). Here we present an examination of MY 24–25 Mars Orbiter Camera (MOC) dust storms and MY 24–26 transient baroclinic eddies identified from Fast Fourier Mapping (FFSM) (Barnes 2001, 2003, 2006) of Thermal Emission Spectrometer (TES) temperatures (Smith 2004), corresponding to the first two phases of the MY 25 storm: precursor,  $L_s=176.2\text{--}184.7^\circ$ , and expansion,  $L_s=184.7\text{--}193^\circ$ .

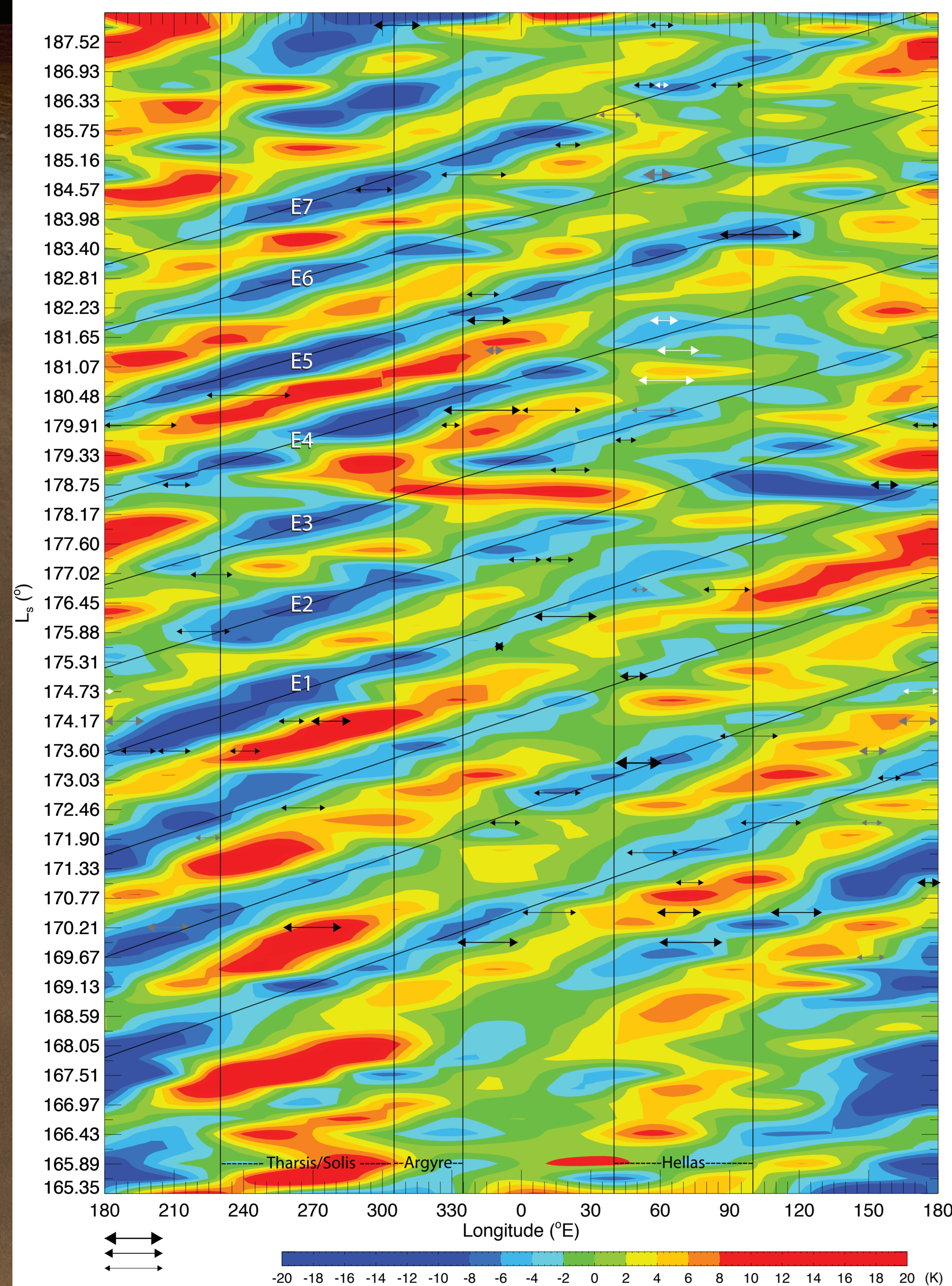


**Fig. 1** - MY 24 TES FFSM 3.7 hPa 60° S eddies and MOC storms. Color = storm central latitude: black < 45° S, grey 35–45° S, and white 25–35° S

## Results

Figures 1, 3, & 4 are longitude-time plots of TES 3.7 hPa temperature anomalies at 60° S for MY 24–26. Figures 1 and 3 compare eddies and dust storms from  $L_s=165\text{--}188^\circ$  during MY 24 and 25 respectively. Arrows delimit the longitudinal extent of dust storms based on our analysis of MOC images provided by MSSS and Cantor (2007). Three arrow sizes represent a subjective magnitude scale of apparent convective activity/structure. Figure 2 shows FFSM eddies on MOC imagery in the Hellas quadrant at  $L_s=177.5^\circ$ . A large cap-edge storm is visible in the SW corner of the Hellas Basin.

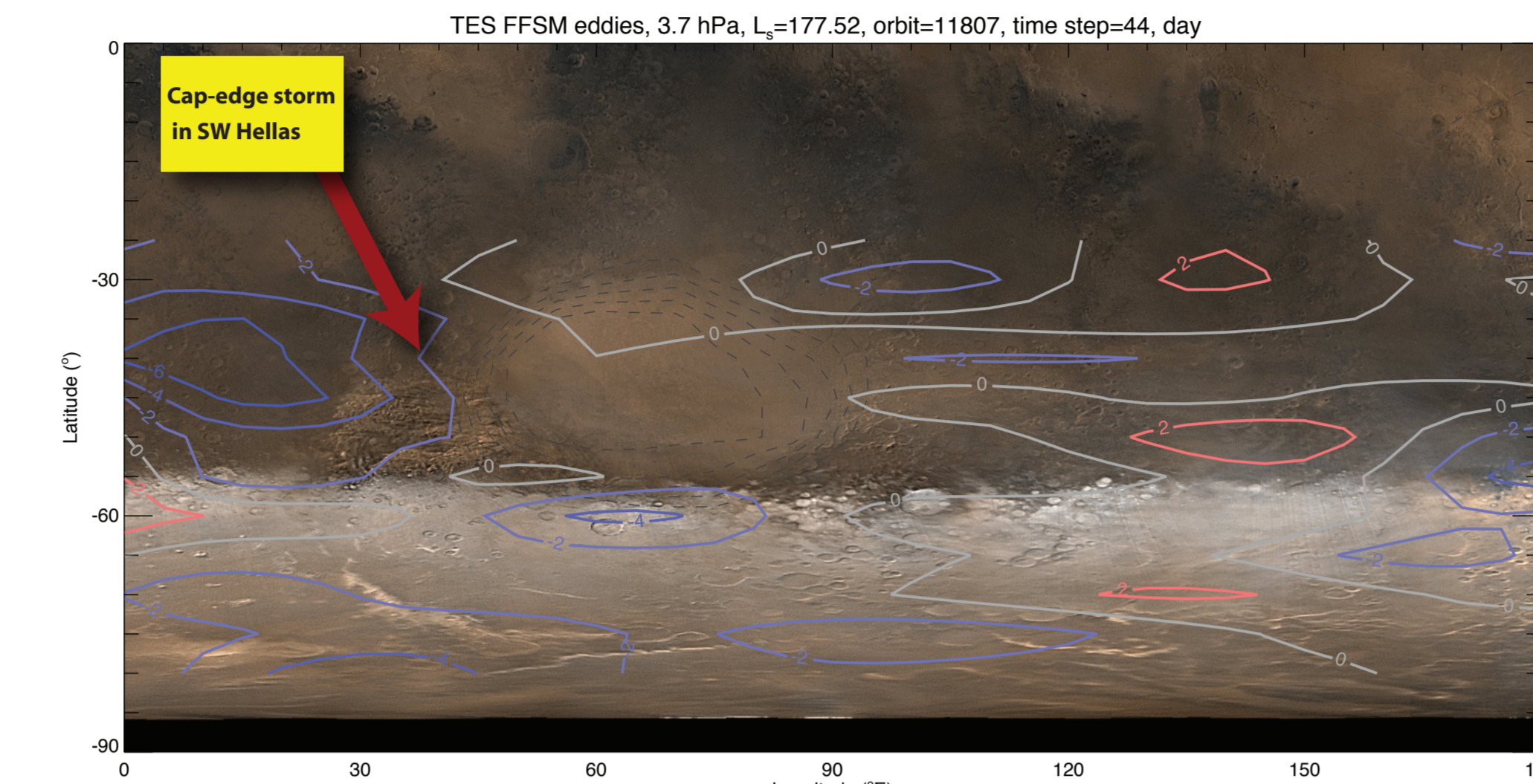


**Fig. 2** - TES 3.7 hPa FFSM eddies on MOC, Hellas quadrant,  $L_s=177.52$ . Image courtesy Malin Space Science Systems

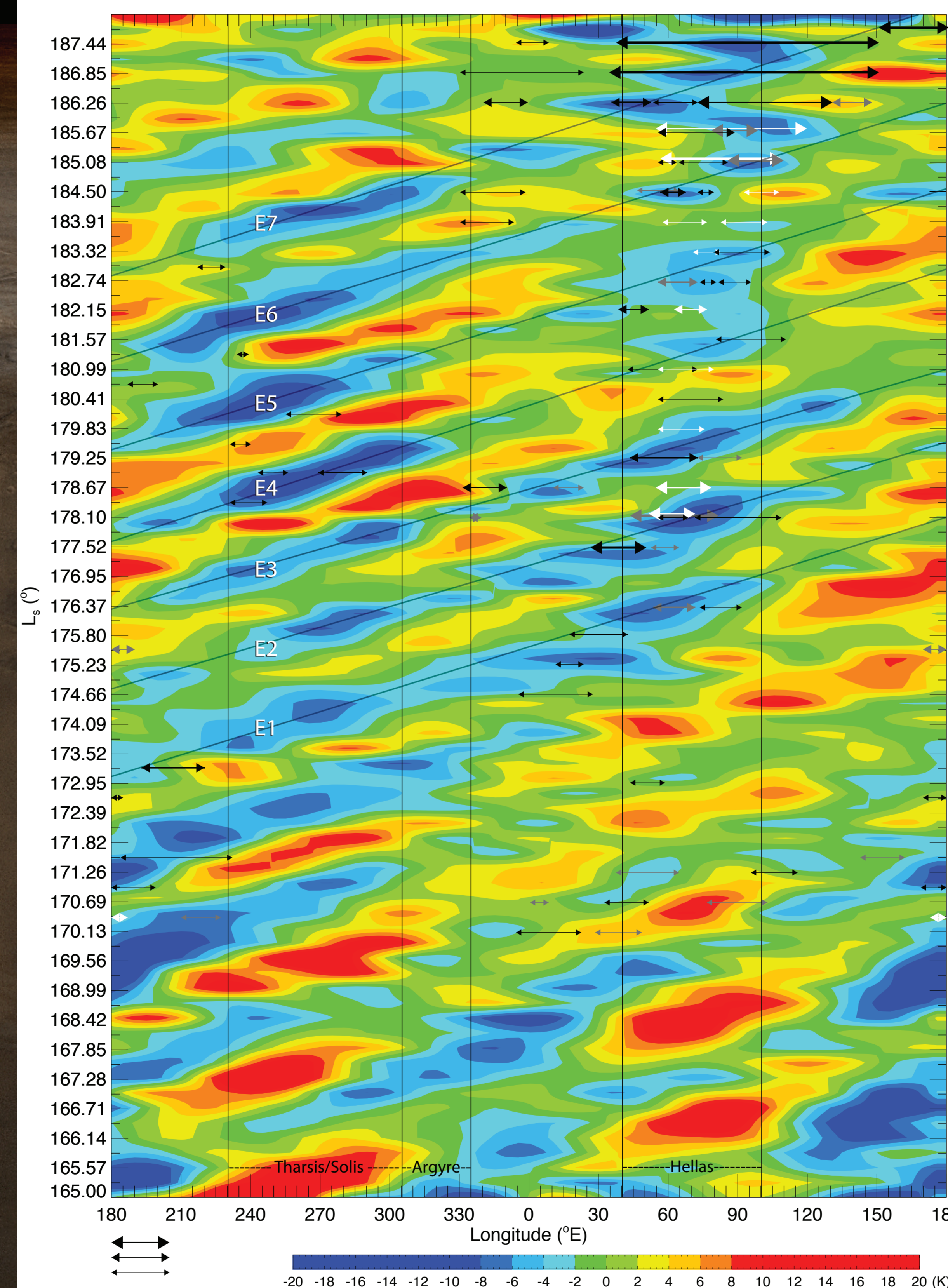


**Fig. 3** - MY 25 TES FFSM 3.7 hPa 60° S eddies and MOC storms

**Transient eddies and storm genesis:** FFSM analysis of TES MY 25 temperatures (Barnes 2006) show that seven cold centers (E1–E7) originated in the Tharsis hemisphere and then propagated through Hellas ~four sols later from  $\sim L_s=174\text{--}187^\circ$ , assuming that they are coherent (or nearly so) from  $200\text{--}90^\circ$  E (Fig. 3). The first eddy (E1) originated near  $230^\circ$  E at  $L_s=173.52^\circ$  and propagated through Hellas from  $\sim L_s=175\text{--}177^\circ$ , corresponding to the first pulse of storm activity described by Cantor (2007).

The cold anomaly passing through Hellas between  $\sim L_s=176\text{--}179^\circ$  appears to be among the largest temporally, spatially, and amplitude during the precursor phase. The corresponding cap-edge storm

at  $L_s=177.5^\circ$  appears to have the most intense convective activity of this phase (Fig. 2).

**Interannual eddy variability MY 24–26:** The data show moderate interannual variability of eddy activity in MY 24 and 25, and significant variability when comparing MY 26 with MY 24 and 25. MY 25 eddies

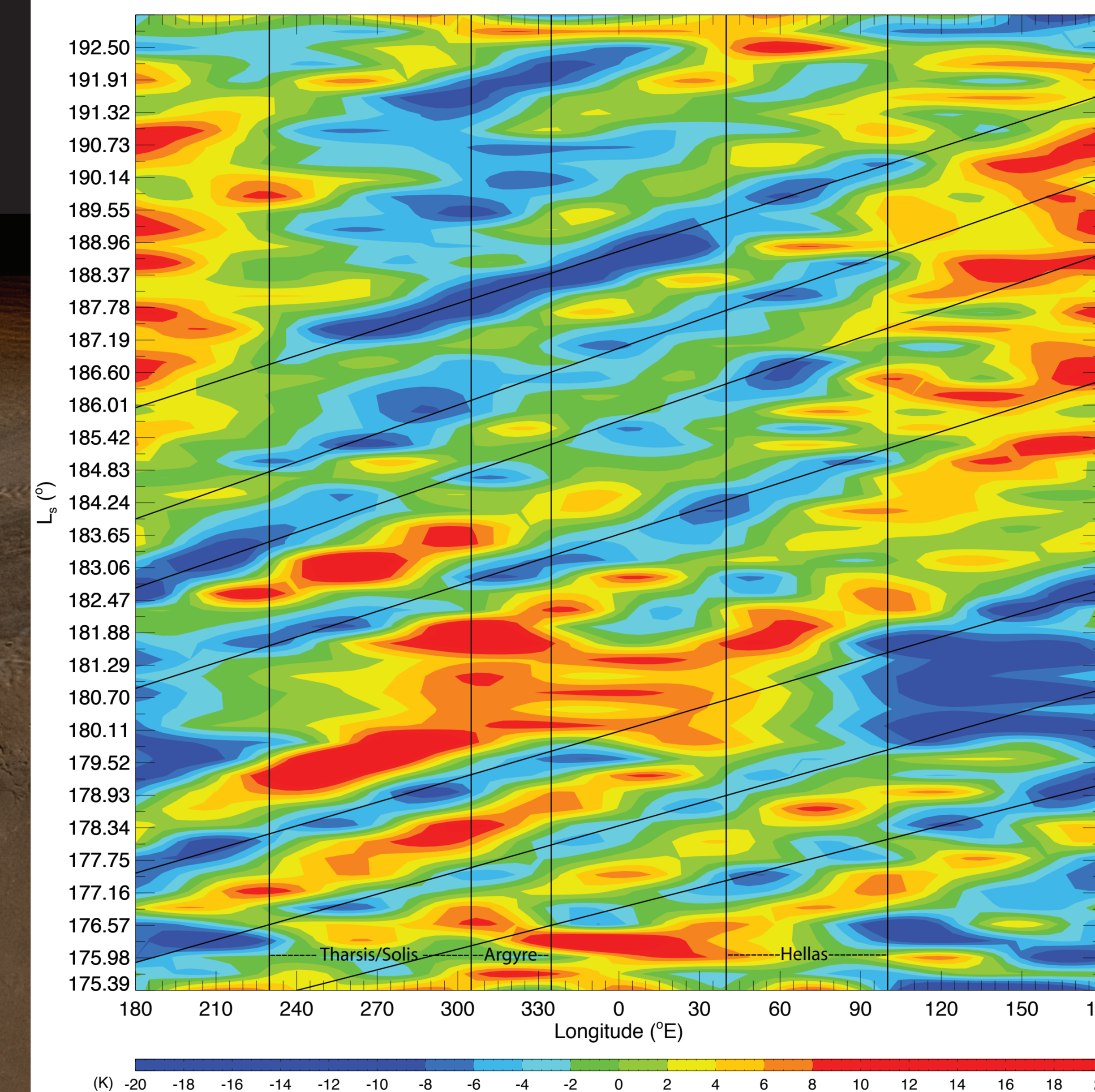


**Fig. 4** - MY 26 TES FFSM 3.7 hPa 60° S eddies

1–3 ( $L_s\sim 175\text{--}179$ ) are relatively high-amplitude in Hellas. Figure 5 shows MY 24–26 FFSM cold anomaly amplitudes vs. time in Hellas ( $45\text{--}90^\circ$  E,  $50\text{--}60^\circ$  S). MY 25 eddies during the precursor phase are moderately stronger amplitude than corresponding MY 24 eddies, and significantly stronger than those in MY 26.

**Phase and Periodicity:** MY 24–26 mean global phase speeds of 14.3, 13.8, 13.7 m/s respectively show that MY 25 eddies were  $\sim 0.5$  m/s slower than those in MY 24. Mean eddy periodicity in Hellas ( $60^\circ$  E) was 2.7, 2.9, and 3.1 sols for MY 24–26 respectively.

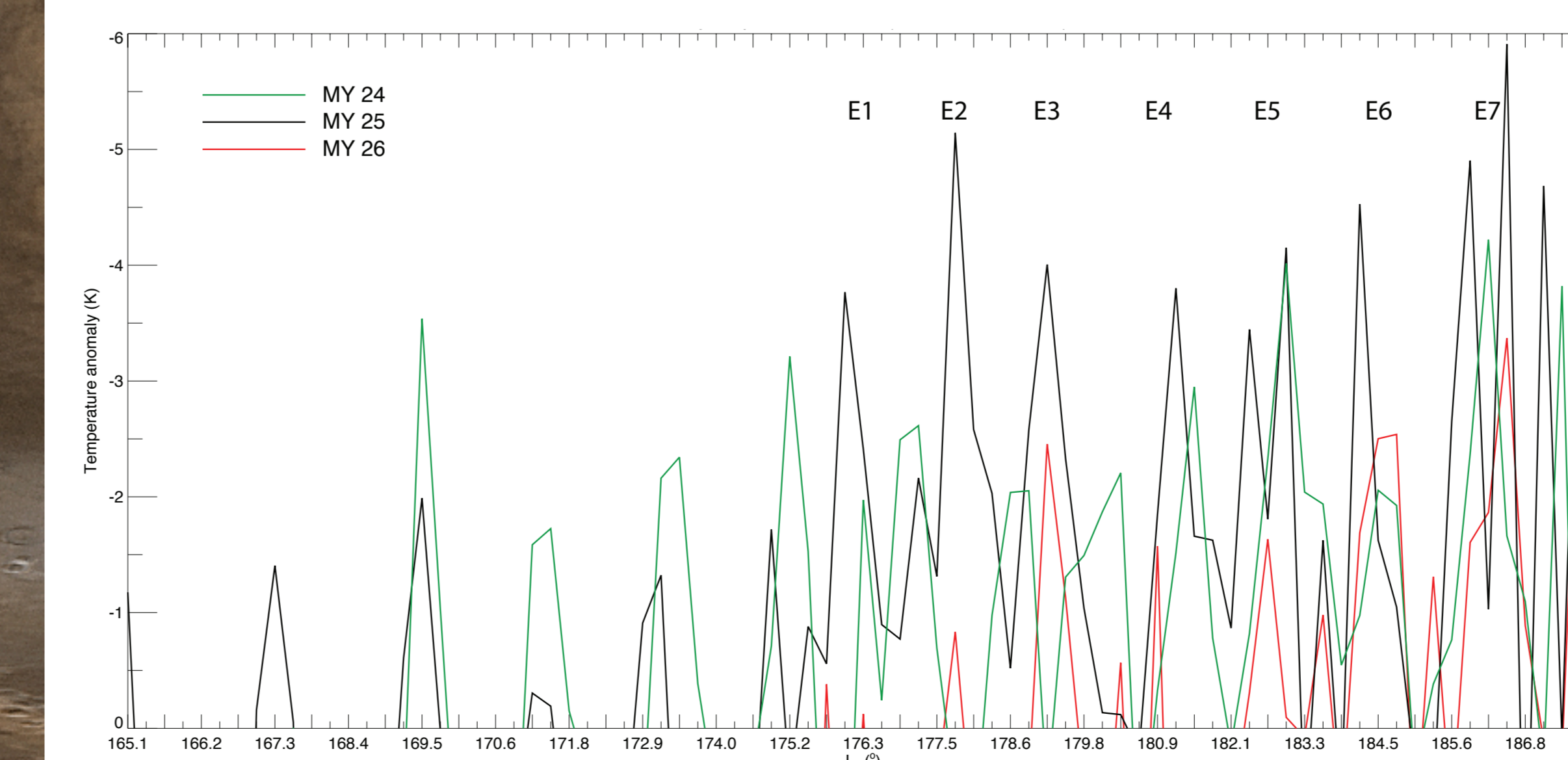


**Fig. 5** - Evolution of TES FFSM 3.7 hPa cold anomaly amplitudes in Hellas ( $45\text{--}90^\circ$  E,  $50\text{--}60^\circ$  S)

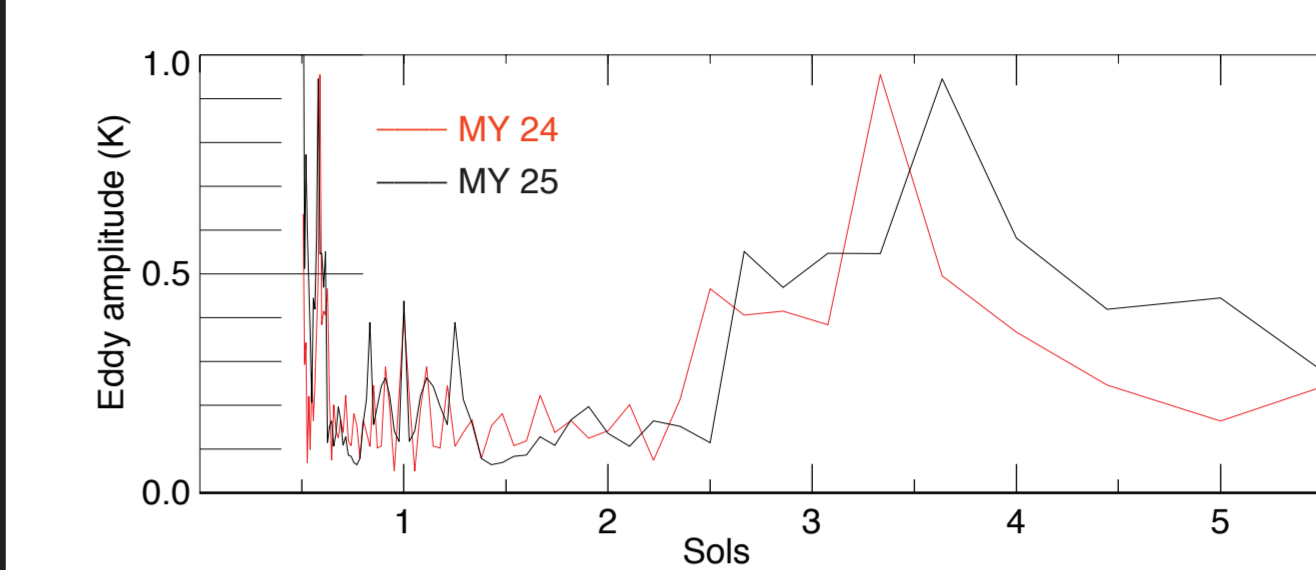


**Fig. 6** - FFT power spectra of Hellas eddies ( $40\text{--}100^\circ$  E,  $60^\circ$  S),  $L_s=165\text{--}188^\circ$ , MY 24–25

FFT Fast Fourier Transform (FFT) power spectra (Fig. 6) show a dominant periodicity of  $\sim 3.5$  sols for both years and values, along with moderately high adjacent amplitudes at  $\sim 2.8$  sols. Since there are 80 time steps (40 sols), wave 13 is 6.2 sols, and wave 14 is 5.7. Wave number resolution and heterogeneous data contribute to the wide, moderate-amplitude ( $\pm 0.5$  K) spread from 2.5–4 sols. FFT power spectra of negative values at  $\sim 3.5$  sols show  $\sim$ twice the amplitude in MY 25 compared with MY 24.

## Conclusions

Integration of FFSM and MOC MY 24 and 25 data shows interesting temporal and spatial associations between the evolution of eddies and storms, including: 1) comparable periodicities of travelling waves and pulses of storm activity; 2) concurrent eastward propagation of both eddies and storms; and 3) location of high-latitude storms on the leading (eastern) of eddies. These results suggest a causal relationship between baroclinic eddies and local storm initiation.

Figure 2 shows storms emerging on or near the leading edges of strong-amplitude cold centers during the MY 25 precursor phase. Figures 1 and 3 show a spatial and temporal correlation between eastward eddy propagation and eastward storm evolution. This relationship is visible in MY 24 storm sequences (Fig. 1) starting at  $L_s=169.9^\circ$  ( $330$  and  $60^\circ$  E),  $L_s=172.7^\circ$  ( $0^\circ$  E), and  $L_s=184.57^\circ$  ( $290^\circ$  E), and also in most MY 25 sequences (Fig. 3), especially as eddies 1, 2, 3, 5, and 6 propagate through Hellas. A northward storm evolution is visible as eddies 2 and 5 pass through Hellas at  $\sim L_s=178$  and  $182^\circ$  during MY 25.

We hypothesize that baroclinic eddies played a significant role in triggering the MY 25 precursor phase regional storms. Determining the factors responsible for PDS genesis in MY 25 and not 24 and 26 is difficult. MY 24–26 Hellas periodicities of 2.7, 2.9, and 3.1 sols respectively show minor interannual variability, as well as global phase speeds of 14.3, 13.8, and 13.7 m/s. The most notable difference is the amplitude of E1–E7 eddies in Hellas (Fig. 5), with all seven MY 25 eddies colder than  $\sim -3.5$  K, compared with two (or three) in MY 24 and one (or two) in MY 26. It is possible that the sustained series of high-amplitude eddies in MY 25 was a factor in PDS interannual variability. If other interannual differences in transient eddy activity were involved in MY 25 PDS genesis, then they may be features undetectable by TES, such as very shallow disturbances. Non-dynamical factors possibly governing PDS interannual variability include dust sources and sinks.

Constructive interference of transient eddies and other circulation components in MY 25, including sublimation flow, anabatic winds (daytime upslope), diurnal tides, and dust-induced thermal tides, may have led to the initiation, amplification, and sustained expansion of precursor storms. Constructive interference increases surface stresses capable of lifting dust. Dust suspended during the precursor phase greatly amplified thermal tides, that in turn contributed to greater storm growth within, and expansion out of Hellas, compared to other years.

References available in *Mars Atmosphere*, Paris 2011 abstract